Journal of Catalysis 397 (2021) 183–191

Contents lists available at ScienceDirect

Journal of Catalysis

journal homepage: www.elsevier.com/locate/jcat

Characterization of Pt-based oxidation catalyst – Deactivated simultaneously by sulfur and phosphorus

Mari Honkanen [a,*], Mika Huuhtanen [b], Marja Kärkkäinen [b], Tomi Kanerva [c], Kimmo Lahtonen [d], Ari Väliheikki [b,e], Kauko Kallinen [e], Riitta L. Keiski [b], Minnamari Vippola [a,f]

[a] Tampere Microscopy Center, Tampere University, P.O. Box 692, 33014 Tampere University, Finland
[b] Environmental and Chemical Engineering, University of Oulu, P.O. Box 4300, 90014 University of Oulu, Finland
[c] Finnish Institute of Occupational Health, P.O. Box 40, 00032 Työterveyslaitos, Finland
[d] Faculty of Engineering and Natural Sciences, Tampere University, P.O. Box 692, 33014 Tampere University, Finland
[e] Dinex Finland Oy, Vihtavuorentie 162, 41330 Vihtavuori, Finland
[f] Faculty of Engineering and Natural Sciences, Materials Science and Environmental Engineering, Tampere University, P.O. Box 589, 33014 Tampere University, Finland

ARTICLE INFO

Article history:
Received 22 December 2020
Revised 19 March 2021
Accepted 22 March 2021
Available online 31 March 2021

Keywords:
Deactivation
Environmental catalysis
Analytical transmission electron microscopy
Fourier transform infrared spectroscopy
X-ray photoelectron spectroscopy

ABSTRACT

Simultaneous poisoning of sulfur + phosphorus on a platinum-based diesel oxidation catalyst was studied to gain a deeper understanding on the catalyst deactivation. Compared to a single poisoning (sulfur or phosphorus), the simultaneous poisoning had a severe effect on the catalyst activation: light-off temperature for 90% conversion of propene was not reached, this of carbon monoxide was much higher than expected, and the maximum conversion of nitrogen monoxide collapsed. With very comprehensive structural characterization by various methods (e.g. STEM-EDS, XPS, DRIFTS) used, we achieved to conclude an explanation for this. In the case of the S + P-poisoning of the catalyst, formed aluminum phosphate was found to block adsorption sites for sulfur species on alumina and sulfur adsorbs mainly on cerium oxides. In addition, sulfur species remain with and in the vicinity of the platinum particles blocking active sites.
© 2021 The Author(s). Published by Elsevier Inc. This is an open access article under the CC BY-NC-ND license (http://creativecommons.org/licenses/by-nc-nd/4.0/).

1. Introduction

An exhaust gas purification system in a diesel engine consists of a diesel oxidation catalyst (DOC), a particulate filter, and a nitrogen oxides (NO_x) storage catalyst or a selective catalytic reduction (SCR) system [1]. The function of the DOC is to oxidize CO and HC to CO_2 and water and to oxidize NO to NO_2 [2,3]. Pt-based catalysts, working at low temperatures (190–250 °C) [4], are widely used in the exhaust aftertreatment systems in diesel engines and alumina is the most common support material used [3].

Performance of the catalysts decreases over the time; thus, to extend a catalysts lifetime, it is important to study deactivation phenomena. Catalytic converters have been used since the 1970s in vehicles and stationary applications, however, their deactivation is still a major problem and it is not fully understood. In the thermal deactivation, the active surface area of the catalyst decreases because of structural changes of the catalyst support and/or active metal sites. In the poisoning, the active surface area of the catalyst decreases because poisoning elements will chemisorb and foul the active metal or support surface preventing the desired reactions [3]. The deactivation of DOCs by sulfur is one of the most important challenges in the diesel engine exhaust aftertreatment [5]. Sulfur originates from low-quality fuels and lubricants and even a very small amount of sulfur can decrease the performance of the catalyst [6]. Under oxygen-rich conditions in the diesel engine, sulfur compounds are oxidized to SO_2 followed by oxidation to SO_3 on the Pt particles in the DOC [7,8]. In the presence of oxygen, platinum is the very active catalyst oxidizing SO_2 to SO_3, and the reaction starts already at ~ 150 °C [9,10]. However, the formation of platinum sulfate is not favored [4] and formed SO_3 strongly interacts with the support components, e.g. alumina, ceria, and ceria + zirconia, forming metal sulfates [11,12]. $Al_2(SO_4)_3$ starts to form at 600 °C and is catalyzed by Pt. $Ce(SO_4)_2$ forms at 195 °C [11]. Thus, Pt improves the storage of sulfur into sulfating supports oxidizing sulfite to sulfate [3]. For example, in the case of the alumina support, formed $Al_2(SO_4)_3$ covers the alumina surface and/or plug its micropores [8]. Sulfur species are formed on ceria and mixed ceria + zirconia also without Pt because they are able to oxidize SO_2 without any catalyst [12]. CeO_2-based materials can be

* Corresponding author.
E-mail addresses: mari.honkanen@tuni.fi (M. Honkanen), mika.huuhtanen@oulu.fi (M. Huuhtanen), marja.karkkainen@oulu.fi (M. Kärkkäinen), tomi.kanerva@ttl.fi (T. Kanerva), kimmo.lahtonen@tuni.fi (K. Lahtonen), avh@dinex.fi (A. Väliheikki), kki@dinex.fi (K. Kallinen), riitta.keiski@oulu.fi (R.L. Keiski), minnamari.vippola@tuni.fi (M. Vippola).

https://doi.org/10.1016/j.jcat.2021.03.026
0021-9517/© 2021 The Author(s). Published by Elsevier Inc.
This is an open access article under the CC BY-NC-ND license (http://creativecommons.org/licenses/by-nc-nd/4.0/).

used as a NO_x storage and release component and may having some promotion effect on the light-off performance and selectivity in the DOC and thus, the sulfation of CeO_2 decreases the catalyst performance [13]. In addition of sulfur, it is known that phosphorus, originating e.g. from lubricating oils, deactivates Pt-based catalysts [14]. Because of affinity between Al and P, they will form dense and amorphous $AlPO_4$ in the case of the alumina-based support [15,16]. Phosphate overlayers cause fouling of the support surface, clogging of the pores, and occlusion of the noble metal particles decreasing significantly the catalyst performance [13,17–19].

Sulfur and phosphorus adsorb differently onto the catalyst monoliths. Sulfur goes mainly uniformly throughout the catalyst length and support depth [14,20,21], while, phosphorus exists mainly in the inlet part of the catalyst monolith and on the top layer of the support [14,17,18,22,23]. Beckman et al. [14] have noticed that ~ 5% of sulfur fed into the system was absorbed in the catalyst after the poisoning treatment. The amount of sulfur in the catalyst depended on the sulfur content in fuel (increasing with increasing sulfur content). In addition, the amount of sulfur depended also on the phosphorus content (increasing with decreasing phosphorus content). The phosphorus content in the catalyst depended directly on its amount in the lubricating oil and even 70% of the amount of phosphorus in the system could be found from the catalyst. Buwono et al. [13] have studied the adsorption of SO_2 and phosphorus oxides on the Rh/Al_2O_3 and $Rh/AlPO_4$ catalysts. They reported that nearly all SO_2 in the gas feed was adsorbed on the Rh/Al_2O_3 until a saturation point was reached. While, only a very small amount of SO_2 was adsorbed on the $Rh/AlPO_4$ because of the lack of basic sites on the surface of $AlPO_4$ were present. Phosphorus oxides formed amorphous $AlPO_4$ layers with Al_2O_3 while the $AlPO_4$ surface was less reactive with sulfur oxides.

In our earlier studies [18,21], we have noticed that sulfur or phosphorus presenting in the catalyst decreases the performance of the Pt-based DOCs. Here, we observed that the simultaneous sulfur + phosphorus poisoning causes more severe deactivation than sulfur and phosphorus separately. In addition, their interaction with catalyst components varies depending on the existence of sulfur only or both sulfur and phosphorus. With very comprehensive structural characterization by various methods, we achieved to conclude an explanation for this. Thus, in the laboratory-scale accelerated poisoning tests, it is very important to use co-treatments to simulate the real conditions wherein many poisoning elements exist at the same time. Based on our knowledge, only in a few articles [24,25] the co-effect of sulfur and phosphorus on the catalyst performance by accelerated laboratory-scale tests has been studied. In our earlier article [25], the DOC studied was Pt/SiO_2-ZrO_2, thus with very different support material than here we have studied. Dahlin et al. [24] have studied the co-effect of sulfur and phosphorus on the SCR catalysts (Cu-SSZ-13 and V_2O_5-WO_3/TiO_2).

2. Material and methods

A catalyst studied was a metallic DOC containing platinum (50 g/cft) supported on the alumina-based washcoat including additives (Ti, Ce, Si, and Zr oxides). It was provided by Dinex Finland Oy (formerly Ecocat Oy). The inlet and outlet part of the catalyst was studied as fresh and after laboratory-scale accelerated phosphorus and sulfur treatments (Fig. 1). In the treatment, the catalyst was placed in a vertically positioned tubular quartz reactor, and the total flow was 1 dm^3/min and the gas hourly space velocity (GHSV) was 21 000 h^{-1} [25]. The sample (marked as PSW) was poisoned for 5 h at 400 °C. The feed contained 10% H_2O with phosphorus c($(NH_4)_2HPO_4$) = 0.13 M (solution fed by a peristaltic pump), and 100 ppm SO_2, 10% air, and N_2 balancing

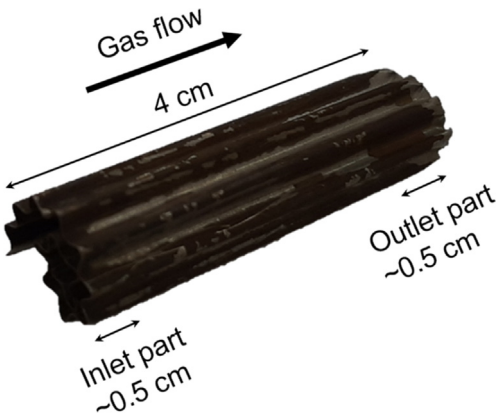

Fig. 1. The photo of the catalyst sample.

gas. The PSW-treated sample was compared to a water-treated (marked as W) [18] and to single phosphorus- (marked as PW) [16,18] and sulfur- (marked as SW) [21] treated samples to deeply understand the co-effects of phosphorus and sulfur. The PW and SW treatments were carried out similarly than the PSW treatment, just leaving out SO_2 and $(NH_4)_2HPO_4$, respectively, and the W treatment leaving out both SO_2 and $(NH_4)_2HPO_4$. The accelerated laboratory-scale treatments used in this study have been developed and validated against the information achieved from the catalysts used in the real conditions [17,21,22]. Thus, the used treatment conditions have been selected so that the amount of poisons in the laboratory-scale-treated catalysts corresponds with the analyzed values from the real ones.

Laboratory-scale diesel oxidation activity measurements were carried out for the PSW-treated catalyst in lean reaction conditions using the following gas mixture: 1000 ppm NO, 500 ppm CO, 300 ppm C_3H_6, 12 vol% O_2 and 10 vol% H_2O, and N_2 as balance gas. The total gas flow was 1 dm^3/min, resulting in a gas hourly space velocity (GHSV) of 31,000 h^{-1} for a monolith. The measurements were carried out at atmospheric pressure in a horizontally aligned tubular quartz reactor. The temperature was increased from room temperature up to 300 °C with a linear heating rate of 5 °C/min under the reaction gas mixture flow H_2O adding was started at 110 °C with a peristaltic pump. The catalyst was kept in a steady state for 15 min at 300 °C, and after that, the furnace was cooled down to room temperature under the N_2 flow. The procedure was repeated twice to determine the repeatability. Gas flow rates were controlled by mass flow controllers (Brooks 5280S). The outlet gas composition was measured by a GasmetTM FT-IR gas analyzer. Oxygen concentration was determined with a paramagnetic oxygen analyzer (ABB Advanced Optima).

The catalyst samples were characterized at microscale by a field emission scanning electron microscope (FESEM, Crossbeam 540, Zeiss) equipped with an energy dispersive spectrometer (EDS, XMaxN silicon drift detector, Oxford Instruments). For imaging, an energy selective backscattered (EsB) detector was used to maximize a compositional contrast. Cross-sectional samples for FESEM studies were prepared by a conventional metallographic method including molding the sample to resin followed by grinding and polishing and finally by carbon coating to avoid a sample charging during the FESEM-EDS studies. The catalyst samples were studied at nanoscale by a cold field emission gun (scanning) transmission electron microscope ((S)TEM, JEM-F200, Jeol) equipped with EDS (dual EDS system for F200, Jeol). For imaging, a STEM dark field (DF) detector was used to maximize a compositional contrast. STEM samples were prepared by scraping the surface layer of the catalyst material from the monolith followed by crushing the scraped catalyst powder between two laboratory glass slides and

dispersing the powder with ethanol onto a copper grid with a holey carbon film. The scraped catalyst powder was also used for X-ray diffraction analysis (XRD, Empyrean with PIXcel3D detector, PANanalytical, using Cu Kα radiation with wavelength 0.15418 nm). Phases were identified from XRD patterns using the database (PDF-4+ 2020) from International Centre for Diffraction Data (ICDD).

The state of the elements in the catalysts was studied by X-ray photoelectron spectroscopy (XPS). The lens-defined selected-area XPS (SAXPS) was performed employing non-monochromatized broad illuminating DAR400 X-ray source (AlKα, 1486.6 eV, 300 W) and Argus hemispherical electron spectrometer (Omicron Nanotechnology GmbH) equipped with micro-channel plate electron multipliers and a 128 channel stripe anode detector. The core level spectra were collected in normal emission angle with a pass energy of 20 eV, high magnification lens mode, and in-lens aperture yielding circular analysis area of 2.93 mm2 (∅1.93 mm). The surface composition was identified by analyzing core level spectra using CasaXPS software (Version 2.3.19 PR 1.0) [26]. Due to surface charging, the binding energy scale was calibrated according to C 1s C–C/H peak at 284.8 eV. The background subtracted XPS peaks were least-squares fitted with a combination of G–L component line shapes. The relative atomic concentrations were calculated using Scofield photoionization cross sections and an experimentally measured transmission function of the Argus analyzer.

The specific surface area, pore size, and pore volume of the PSW-treated catalyst were measured using the Micrometrics ASAP 2020. Specific surface areas were determined from the N2 adsorption isotherms at −196 °C (77 K) according to the standard Brunauer-Emmet-Teller (BET) method. Pore size and pore volume distributions of the catalysts were calculated from N_2 desorption isotherms by the Barret-Joyner-Halenda (BJH) method.

Table 1
Light-off temperatures for 90% conversions (T_{90}) and maximum NO conversion over the PSW-treated catalyst compared to the fresh, W-, SW-, and PW-treated catalysts.

	T_{90} [°C]		Max conversion [%]
Catalyst	**C_3H_6**	**CO**	**NO**
Fresh [18]	186	160	50
W-treated [18]	192	172	48
SW-treated [21]	206	182	46
PW-treated [18]	295	196	17
PSW-treated [this study]	Not reached	230	6

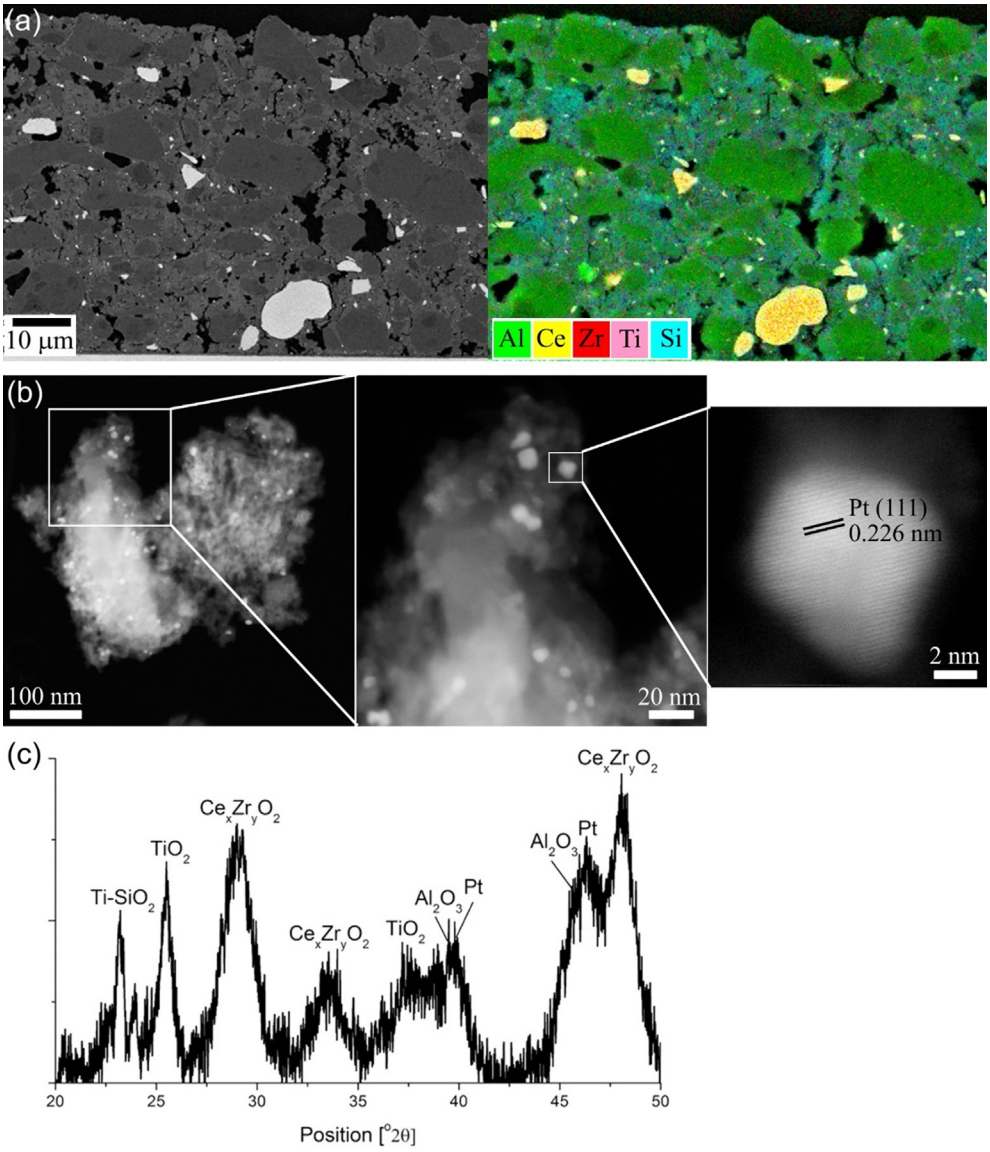

Fig. 2. The fresh catalyst, (a) the cross-sectional FESEM image (EsB) and the layered FESEM-EDS map, (b) the STEM DF images, and (c) the XRD pattern.

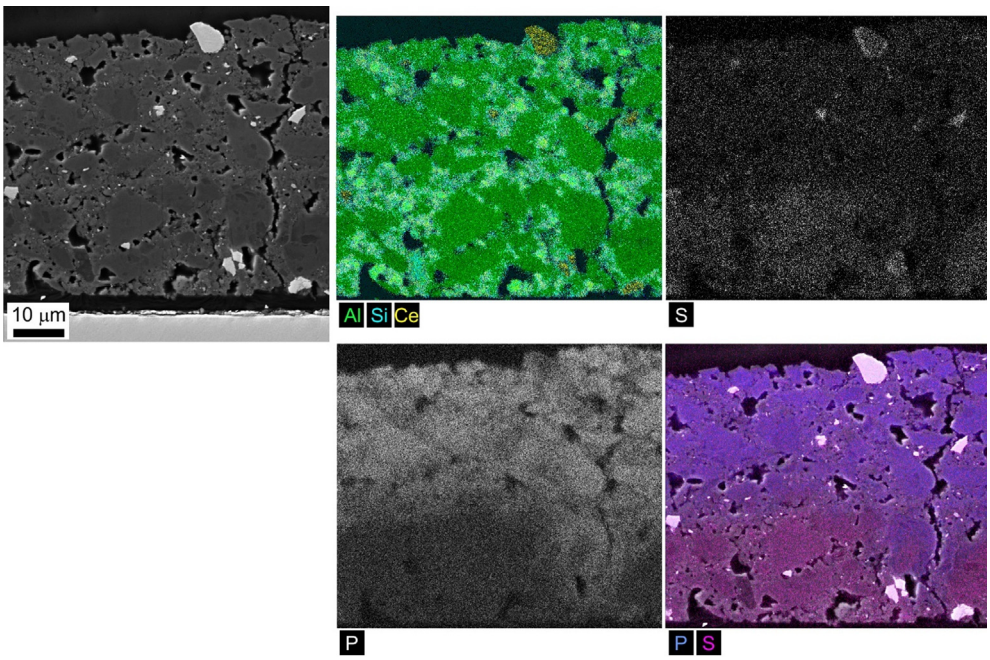

Fig. 3. The cross-sectional FESEM image (EsB) and FESEM-EDS maps from the inlet part of the PSW-treated catalyst. More color indicates higher amount.

A Fourier transform infrared (FT-IR) spectrometer (Bruker, Vertex V80) equipped with a diffuse reflectance infrared Fourier transform (DRIFT) unit (Harrick) and a liquid-nitrogen-cooled mercury cadmium telluride (MCT) detector was utilized to study poisoning compounds on the scraped catalyst sample. The DRIFT measurements were carried out at room temperature under ambient atmosphere conditions. A background spectrum was measured using a mirror. Spectra were recorded by using a resolution of 4 cm^{-1}.

3. Results and discussion

3.1. Effect of sulfur and phosphorus on catalyst performance

The activity test over the PSW-treated catalyst was carried out. In our earlier studies [18,21], the effect of water and single poisons (S and P) on the performance of the DOC studied (CO, C_3H_6 and NO oxidation) has been investigated (Table 1). In the case of the PSW-treated DOC, it was found that light-off temperature for 90% conversion (T_{90}) of C_3H_6 was not reached and this of CO was much higher than expected (Table 1). In addition, a drastic effect was detected in the maximum conversion of NO. Thus, the results indicate that in the presence of both impurities (S and P) simultaneously, a severe catalyst deactivation occurred. However, the reason or mechanism has not been yet clearly explained. Therefore, several characterization methods were used to find out the poisoning mechanism.

3.2. Fresh catalyst

To study the effect of sulfur and phosphorus on the catalyst, it was essential to comprehensively characterize the fresh catalyst. The cross-sectional FESEM image (EsB) and the FESEM-EDS layered elemental map are presented in Fig. 2a. The catalyst consisted of aluminum-rich areas, cerium-rich particles, and titanium and silicon containing areas. Pt particles were too small to be detected by FESEM. The STEM DF images with various magnifications are presented in Fig. 2b showing Pt particles which lattice fringes correspond to metallic Pt. Sequential tilt-series STEM DF images (±55°, in steps of 2°) were collected from the fresh catalyst and the images were constructed to a video (Video 1), bright spots indicate Pt particles. The XRD (Fig. 2c) and XPS results indicated that Pt particles were as metallic form and support material as oxide form (Pt $4f_{7/2}$ at 70.2 eV and Al $2p_{3/2}$ at 74.6 eV).

3.3. Microscale distribution of sulfur and phosphorus

A cross-sectional FESEM image (EsB) and FESEM-EDS maps collected from the inlet part of the PSW-treated catalyst are presented in Fig. 3. Phosphorus existed mainly on the top of the catalyst support and sulfur in the bottom area. More detailed micro-scale distribution of phosphorus and sulfur was studied by FESEM-EDS line analyses collected from the inlet and outlet parts of the PSW-treated catalyst (Fig. 4). In the inlet part (Fig. 4a), phosphorus amount on the top layer of the catalyst was 10–15 wt% clearly favoring alumina-rich areas. The highest sulfur amount, <5 wt%, was detected on the ceria-rich areas (Fig. 4a). However, in the bottom area of the catalyst where in the amount of phosphorus was small, sulfur (<5 wt%) existed more uniformly in the both ceria- and alumina-rich areas. In the outlet part (Fig. 4b), only a very small amount of phosphorus was detected. Sulfur (<5 wt%) existed thoroughly in the outlet part and it was determined mainly to be in the alumina-rich areas and not as much in the ceria-rich areas (Fig. 4b).

To compare the effect of the single- and co-treatments, FESEM-EDS line analyses were collected also from the SW- and PW-treated catalysts (Supplementary material). In the SW-treated sample, a small amount (<5 wt%) of sulfur existed in the inlet and outlet parts thoroughly and its distribution was uniform regardless of alumina- and ceria-rich areas. In the inlet part of the PW-treated catalyst, phosphorus (10–15 wt%) existed mainly on the top layer of the catalyst support and it seemed to favor alumina-rich areas and avoid ceria-rich areas. Only a very small amount of phosphorus was detected in the outlet part of the PW-treated catalyst. The average amount of phosphorus and sulfur was similar in the both single- and co-treatments and a saturation point seemed to be 10–15 wt% for phosphorus and < 5 wt% for sulfur.

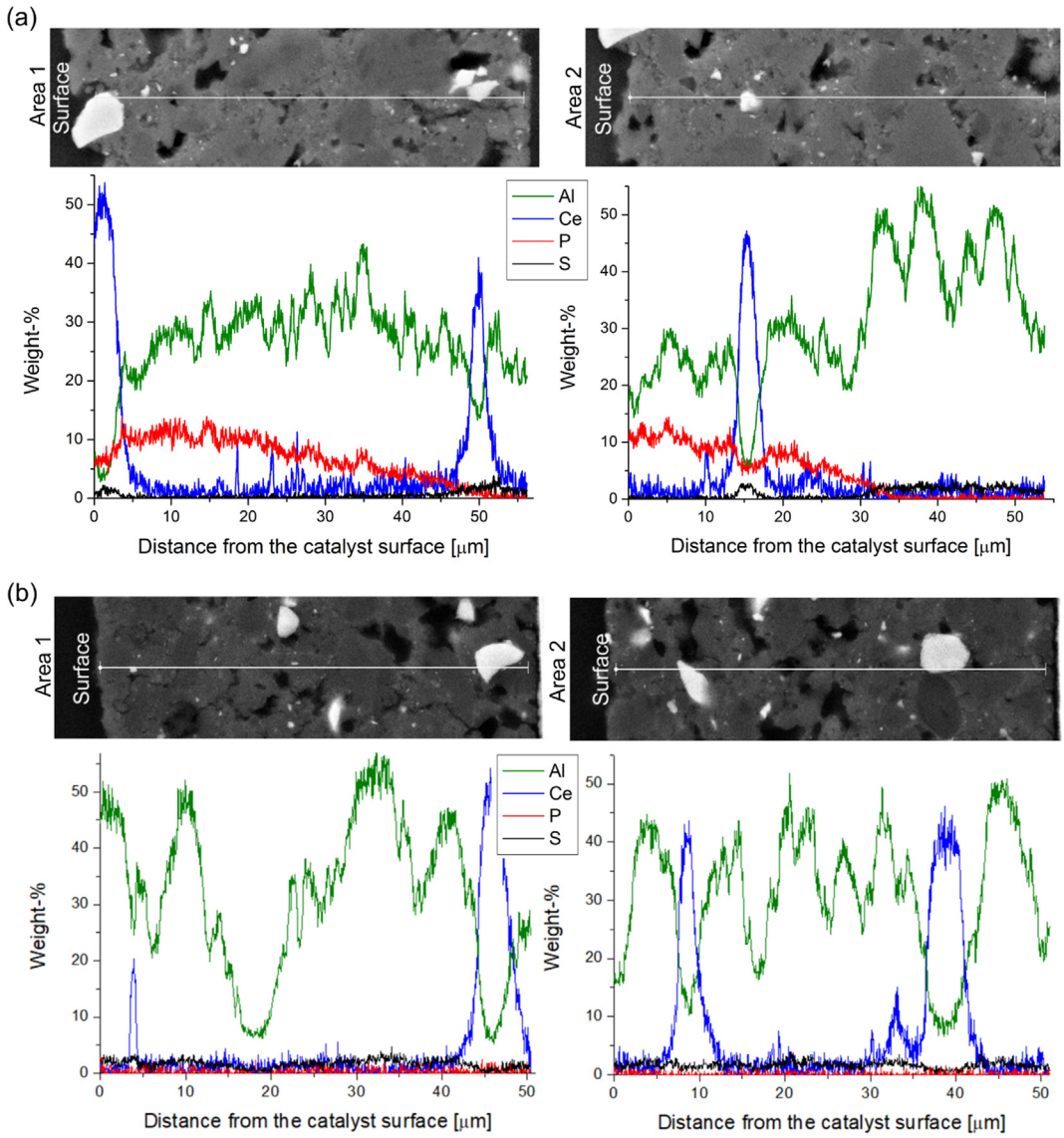

Fig. 4. FESEM-EDS line analyses from the PSW-treated catalyst, (a) two measurement points (areas 1 and 2) from the inlet part and (b) two measurement points (areas 1 and 2) from the outlet part.

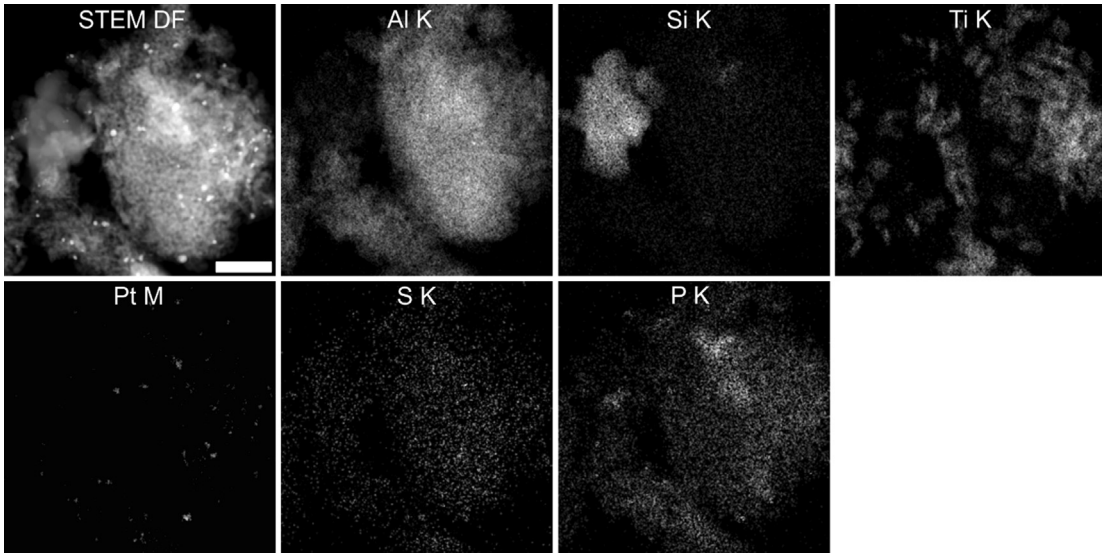

Fig. 5. The STEM DF image and STEM-EDS maps collected from the inlet part of the PSW-treated catalyst. In the maps, brighter color indicates higher amount. Scale bar marked in the STEM DF image is 100 nm.

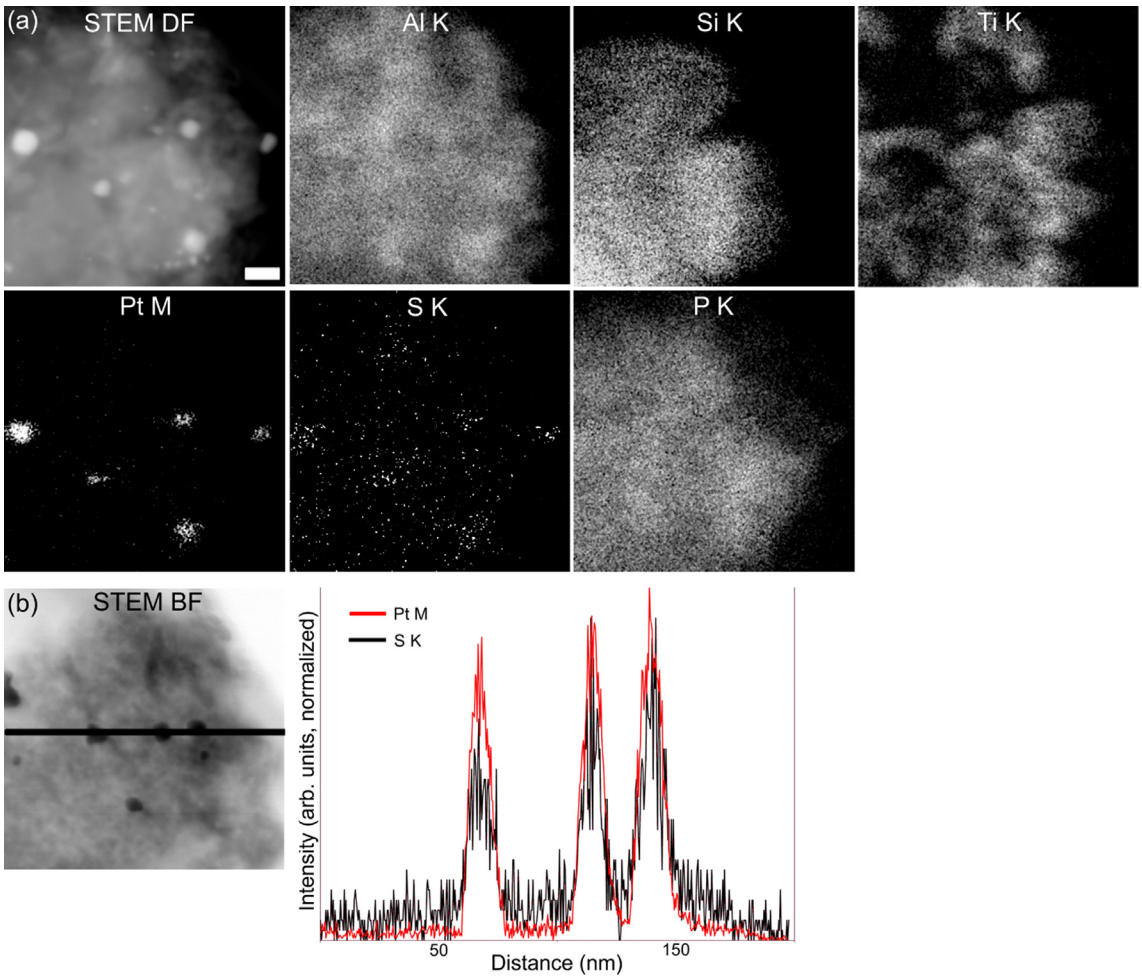

Fig. 6. STEM-EDS results for PSW-treated catalyst. (a) STEM DF image and STEM-EDS maps, brighter color indicates higher amount, scale bar marked in the STEM DF image is 20 nm. (b) STEM BF image and STEM-EDS line analyses over three Pt particles, intensity values for Pt and S are normalized.

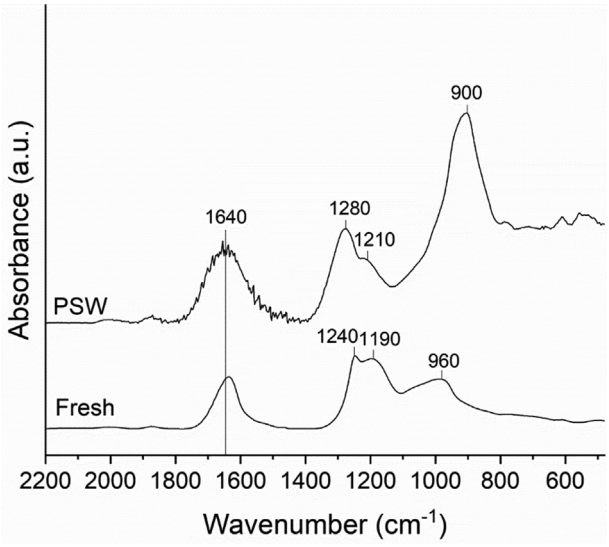

Fig. 7. DRIFT spectra of the fresh and PSW-treated catalysts.

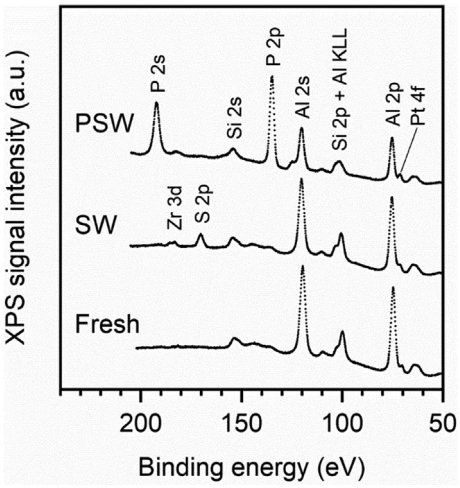

Fig. 8. XPS spectra of the fresh, SW-treated and PSW-treated catalysts.

3.4. Nanoscale distribution of sulfur and phosphorus

To study nanoscale distribution of sulfur and phosphorus after the simultaneous poisoning treatment, STEM-EDS elemental maps were collected from the inlet and outlet parts of the PSW-treated catalyst. By STEM-EDS, it was possible to detect phosphorus also on the top layer of the outlet part of the catalyst although it was challenging to detect with bulk analyses by FESEM-EDS. The STEM-EDS results collected from the inlet and outlet parts of the PSW-treated catalyst were similar. The maps collected from the

Table 2
Crystallite size of Pt particles determined from XRD patterns and particle size determined from STEM images for the fresh, PSW-, PW-, and SW-treated catalysts.

	Fresh	SW inlet	PW inlet	PSW inlet
Crystallite size [nm]	4	4	8	11
Particle size [nm]	6.1 ± 1.8	6.5 ± 1.8	7.2 ± 2.2	6.1 ± 2.4

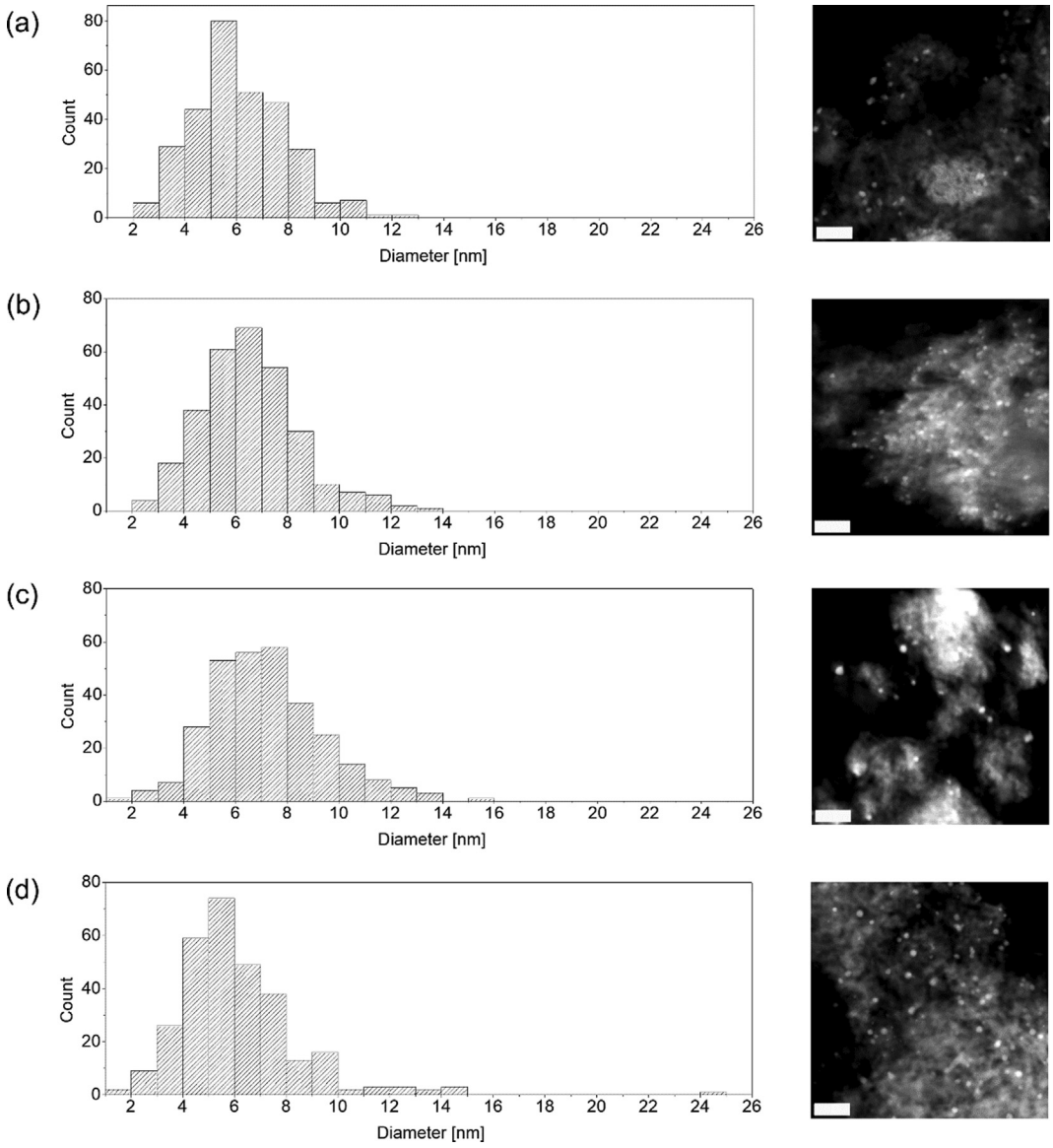

Fig. 9. Histograms and example STEM DF images (bright spots indicate Pt particles, scale bar is 50 nm) showing Pt particle size distributions measured from STEM images (300 particles) for (a) the fresh catalyst, (b) the SW-treated catalyst, (c) the PW-treated catalyst, and (d) the PSW-treated catalyst.

inlet part are presented in Fig. 5: phosphorus seemed to follow alumina-rich areas while sulfur existed all over the catalyst support.

The EDS maps collected from the PSW-treated catalyst with higher magnification than in Fig. 5 are presented in Fig. 6a and line analyses in Fig. 6b: sulfur seemed to locate mainly with and in the vicinity of the Pt particles. Based on the data collected from the SW-treated sample, sulfur existed more uniformly in the support. Phosphorus behaved similarly in the both PW- and PSW-treated samples, favoring aluminum-rich areas. Based on the literature, the deactivation of the noble metal particles is much faster if the support is not adsorbing sulfates and more sulfur species remain on the Pt surface blocking active sites [3]. Adsorption of SO_2 is not favored on the $AlPO_4$ because of the lacking basic sites on the $AlPO_4$ surface [13]. According to our earlier study on a DOC from a heavy-duty vehicle (used for 80 000 km), sulfur followed ceria-rich areas and phosphorus favored alumina-rich areas [22].

3.5. Composition of sulfur and phosphorus

Based on the DRIFT results of the PSW-treated catalyst (Fig. 7), both sulfur and phosphorus species were detected. The peak 1640 cm^{-1} on both fresh and PSW-treated samples is assigned to moisture (–OH) on the catalyst surface e.g. [27]. In the spectrum

of the fresh catalyst, the peaks 960 and 1240 cm^{-1} are due to material vibrations, such as Al-O [28]. The peaks on the PSW-treated sample at 1210–1280 cm^{-1} are assigned as sulfates, most probable O = S = O and O – SO_3 vibrations of $Al_2(SO_4)_3$ [17,20,21,29–32], but 1280 cm^{-1} can be also caused by PO_2 vibration, e.g. [33,34]. In addition, it is challenging to interpret the specific adsorption sites (Al or Ce). In the case of phosphorus, a strong peak at 900 cm^{-1} indicates P – O – P bonds and at 500–650 cm^{-1} as P – O vibrations thus it can be assumed that phosphorus is in the form of phosphates [16,18,33–35]. The gained results are in good agreement with the XPS studies.

According to the XPS measurements (Fig. 8), sulfur was in the form of sulfates on the SW-treated (S $2p_{3/2}$ at 169.8 eV) and PSW-treated (S $2p_{3/2}$ at 169.0 eV) catalyst surfaces. Phosphorus had a high oxidation state on the PSW-treated sample (P $2p_{3/2}$ at 134.6 eV) suggesting phosphate. Platinum was always in the metallic state in the fresh (Pt $4f_{7/2}$ at 70.2 eV), SW-treated (Pt $4f_{7/2}$ at 71.1 eV), and PSW-treated (Pt $4f_{7/2}$ at 71.1 eV) samples (Supplementary material). The observed 0.9 eV difference in the binding energy of Pt $4f_{7/2}$ between the fresh and PSW-treated catalysts suggests changed surrounding of the Pt atoms in the case of PSW, but not actual Pt–O bonding. Pt oxides should be located at higher binding energies, between 72.4 and 74.9 eV. Also, the Pt crystallite/particle size and the degree of crystallinity could affect both the XPS peak position and width. The concentration ratio of Al:P was 1:1 after the PSW treatment indicating that within the XPS sampling depth the surface contained mainly $Al_1P_1O_x$ species, and not anymore pure Al_2O_3. A drastic change was observed in the relative amount of sulfur at the same time. The atomic concentration of S decreased to one tenth from 2.43 at% on the SW-treated catalyst to 0.25 at% on the PSW-treated catalyst. This can be explained either by decreased absolute amount of sulfur caused by reduced adsorption during the poisoning or the sulfur species were mainly buried below XPS sampling depth by $AlPO_x$ layer.

3.6. Effect of sulfur and phosphorus on catalyst morphology

The crystallite size of Pt particles for the fresh catalyst and after the SW-, PW-, and PSW-treatments was determined from the XRD patterns by Scherrer equation (Table 2). Corresponding Pt particle sizes (300 particles) were measured from STEM DF images (Table 2 and Fig. 9) by the TEM Center software (TEM Operation & Acquisition System for JEM-F200). STEM studies indicated that Pt particles were mainly single crystals. Based on the XRD measurements, the Pt crystallite size increased in the PW- and PSW-treatments. According to STEM studies, growing was very slight. Based on the histograms (Fig. 9), in the poisoned catalysts, there were some larger particles compared to the fresh catalyst. However, poisoning treatments caused only a slight Pt particle growing which is not exclusively explaining the severe deactivation of the PSW-treated catalyst.

Specific surface area (S_{BET}), total pore volume, and average pore size of the fresh and treated catalysts are presented in Table 3. The W-treatment had a negligible effect on the catalyst [18]. S_{BET} and total pore volume values decreased in the order of SW- [21], PW- [18] and PSW-treatments, however, the pore sizes remained unchanged regardless of the treatment. BET isotherms (not shown) followed the IUPAC classification type IV(a) indicating material having quite large mesopores with size 2–50 nm [36,37]. Formation of the microporous aluminum phosphate layer on the alumina surface (in the PW- and PSW-treated catalysts) is assumed to influence on the total pore volumes and specific surface area.

Table 3
Specific surface area (S_{BET}), total pore volume, and average pore size for the fresh and treated catalysts.

	Specific surface area [m^2/g]	**Total pore volume** [cm^3/g]	**Average pore size** [nm]
Fresh [18]	225	0.41	7.5
W-treated [18]	218	0.40	7.3
SW-treated [21]	192	0.36	7.6
PW-treated [18]	137	0.26	7.4
PSW-treated [this study]	108	0.20	7.6

4. Conclusions

Catalyst deactivation caused by simultaneous sulfur and phosphorus exposure in the Pt-based catalyst with an alumina-rich support was studied. Compared to a single poisoning (sulfur or phosphorus), the simultaneous poisoning (PSW) caused severe effects on the catalyst activation: the light-off temperature (T_{90}) of propene was not reached, T_{90} of carbon monoxide was higher (30–70 °C) than this of the fresh- and single-element poisoned, and the maximum conversion of nitrogen monoxide collapsed below 10%. By several characterization methods utilized to find out the deactivation mechanism, it can be concluded that phosphorus favors formation of aluminum phosphate. Formed aluminum phosphate acts as a non-sulfating support hindering the migration of sulfur oxides from the Pt particles to the support leading more severe poisoning of the Pt particles. Thus, in the absence of phosphorus, sulfur distributes evenly throughout the catalyst support as aluminum sulfate, but in the presence of phosphorus, sulfur adsorbs mainly on mixed cerium and zirconium oxide. In the case of the PSW poisoning, the support becomes poisoned by both sulfur and phosphorus species, and, in addition, Pt particles are covered by sulfur species. To gain deeper understanding on the catalyst deactivation phenomena, introducing poisoning compounds simultaneously on the catalyst surface is essential.

Declaration of Competing Interest

The authors declare that they have no known competing financial interests or personal relationships that could have appeared to influence the work reported in this paper.

Acknowledgements

Electron microscopy work made use of Tampere Microscopy Center facilities at Tampere University.

Appendix A. Supplementary material

Supplementary data to this article can be found online at https://doi.org/10.1016/j.jcat.2021.03.026.

References

[1] K. Hauff, U. Tuttlies, G. Eigenberger, U. Nieken, A global description of DOC kinetics for catalysts with different platinum loadings and aging status, Appl. Catal. B Environ. 100 (1-2) (2010) 10–18, https://doi.org/10.1016/j.apcatb.2010.07.036.
[2] O. Kröcher, M. Widmer, M. Elsener, D. Rothe, Adsorption and desorption of SOx on diesel oxidation catalysts, Ind. Eng. Chem. Res. 48 (22) (2009) 9847–9857, https://doi.org/10.1021/ie900882p.
[3] A. Russell, W.S. Epling, Diesel oxidation catalysts, Catal. Rev. 53 (4) (2011) 337–423, https://doi.org/10.1080/01614940.2011.596429.
[4] G. Corro, Sulfur impact on diesel emission control- A review, React. Kinet. Catal. Lett. 75 (2002) 89–106, https://doi.org/10.1023/A:1014853602908.
[5] H. Sharma, S. Suib, A. Mhadeshwar, Interactions of sulfur oxides with Diesel Oxidation Catalysts (DOCs), Nov. Mater. Catal. Fuels Process., American Chemical Society, 2013, pp. 117–155 SE–5, https://doi.org/10.1021/bk-2013-1132.ch005.

[6] A.T. Gremminger, H.W. Pereira de Carvalho, R. Popescu, J.-D. Grunwaldt, O. Deutschmann, Influence of gas composition on activity and durability of bimetallic Pd-Pt/Al_2O_3 catalysts for total oxidation of methane, Catal. Today. 258 (2015) 470–480, https://doi.org/10.1016/J.CATTOD.2015.01.034.
[7] A.K. Neyestanaki, F. Klingstedt, T. Salmi, D.Y. Murzin, Deactivation of postcombustion catalysts, a review, Fuel 83 (4-5) (2004) 395–408, https://doi.org/10.1016/j.fuel.2003.09.002.
[8] S. Matsumoto, Y. Ikeda, H. Suzuki, M. Ogai, N. Miyoshi, NOx storage-reduction catalyst for automotive exhaust with improved tolerance against sulfur poisoning, Appl. Catal. B Environ. 25 (2-3) (2000) 115–124, https://doi.org/10.1016/S0926-3373(99)00124-1.
[9] Chapter XII The Oxidation of Sulfur-Containing Inorganic Compounds, Stud. Surf. Sci. Catal. 15 (1983) 365–387. https://doi.org/10.1016/S0167-2991(08)64837-5
[10] M.S. Wilburn, W.S. Epling, Formation and decomposition of sulfite and sulfate species on Pt/Pd catalysts: An SO_2 oxidation and sulfur exposure study, ACS Catal. 9 (1) (2019) 640–648, https://doi.org/10.1021/acscatal.8b0352910.1021/acscatal.8b03529.s001.
[11] D.D. Beck, M.H. Krueger, D.R. Monroe, The impact of sulfur on three-way catalysts: storage and removal, SAE Trans. 100 (1991) 386–399. http://www.jstor.org/stable/44553608.
[12] P. Bazin, O. Saur, J.C. Lavalley, A.M. Le Govic, G. Blanchard, Comparative sulfur storage on Pt catalysts: Effect of the support (CeO_2, ZrO_2 and CeO_2-ZrO_2), Elsevier Masson SAS (1998), https://doi.org/10.1016/s0167-2991(98)80912-9.
[13] H. Buwono, S. Minami, K. Uemura, M. Machida, Surface properties of Rh / $AlPO_4$ catalyst providing high resistance to sulfur and phosphorus poisoning, Ind. Eng. Chem. Res. 54 (2015) 7233–7240, https://doi.org/10.1021/acs.iecr.5b01720.
[14] R. Beckmann, W. Engeler, E. Mueller, B. Engler, J. Leyrer, E. Lox, K. Ostgathe, A new generation of diesel oxidation catalysts, in: Int. Fuels Lubr. Meet, Expo., SAE International, 1992, https://doi.org/10.4271/922330.
[15] R. Munirathinam, D. Minh, A. Nzihou, Effect of support and its surface modifications in cobalt-based Fischer-Tropsch synthesis: Review, Industrial and engineering chemistry research, American Chemical Society 57 (2018) 16137–16161, https://doi.org/10.1021/acs.iecr.8b03850.hal-01923787.
[16] M. Honkanen, M. Kärkkäinen, O. Heikkinen, K. Kallinen, T. Kolli, M. Huuhtanen, J. Lahtinen, R.L. Keiski, T. Lepistö, M. Vippola, The effect of phosphorus exposure on diesel oxidation catalysts-part II: Characterization of structural changes by transmission electron microscopy, Top. Catal. 58 (14-17) (2015) 971–976, https://doi.org/10.1007/s11244-015-0465-y.
[17] M. Honkanen, M. Kärkkäinen, V. Viitanen, H. Jiang, K. Kallinen, M. Huuhtanen, M. Vippola, J. Lahtinen, R. Keiski, T. Lepistö, Structural characteristics of natural-gas-vehicle-aged oxidation catalyst, Top. Catal. 56 (9-10) (2013) 576–585, https://doi.org/10.1007/s11244-013-0017-2.
[18] M. Kärkkäinen, T. Kolli, M. Honkanen, O. Heikkinen, M. Huuhtanen, K. Kallinen, T. Lepistö, J. Lahtinen, M. Vippola, R.L. Keiski, The effect of phosphorus exposure on diesel oxidation catalysts-part I: Activity measurements, elementary and surface analyses, Top. Catal. 58 (14-17) (2015) 961–970, https://doi.org/10.1007/s11244-015-0464-z.
[19] M.J. Rokosz, A.E. Chen, C.K. Lowe-Ma, A.V. Kucherov, D. Benson, M.C. Paputa Peck, R.W. McCabe, Characterization of phosphorus-poisoned automotive exhaust catalysts, Appl. Catal. B Environ. 33 (3) (2001) 205–215, https://doi.org/10.1016/S0926-3373(01)00165-5.
[20] M. Honkanen, J. Wang, M. Kärkkäinen, M. Huuhtanen, H. Jiang, K. Kallinen, R.L. Keiski, J. Akola, M. Vippola, Regeneration of sulfur-poisoned Pd-based catalyst for natural gas oxidation, J. Catal. 358 (2018) 253–265, https://doi.org/10.1016/j.jcat.2017.12.021.
[21] M. Kärkkäinen, M. Honkanen, V. Viitanen, T. Kolli, A. Valtanen, M. Huuhtanen, K. Kallinen, M. Vippola, T. Lepistö, J. Lahtinen, R.L. Keiski, Deactivation of diesel oxidation catalysts by sulphur in laboratory and engine-bench scale aging, Top. Catal. 56 (9-10) (2013) 672–678, https://doi.org/10.1007/s11244-013-0048-8.
[22] T. Kanerva, M. Honkanen, T. Kolli, O. Heikkinen, K. Kallinen, T. Saarinen, J. Lahtinen, E. Olsson, R.L. Keiski, M. Vippola, Microstructural characteristics of vehicle-aged heavy-duty diesel oxidation catalyst and natural gas three-way catalyst, Catalysts. 9 (2) (2019) 137, https://doi.org/10.3390/catal9020137.
[23] M.H. Wiebenga, C.H. Kim, S.J. Schmieg, S.H. Oh, D.B. Brown, D.H. Kim, J.-H. Lee, C.H.F. Peden, Deactivation mechanisms of Pt/Pd-based diesel oxidation catalysts, Catal. Today. 184 (1) (2012) 197–204, https://doi.org/10.1016/j.cattod.2011.11.014.
[24] S. Dahlin, J. Englund, H. Malm, M. Feigel, B. Westerberg, F. Regali, M. Skoglundh, L.J. Pettersson, Effect of biofuel- and lube oil-originated sulfur and phosphorus on the performance of Cu-SSZ-13 and V_2O_5-WO_3/TiO_2 SCR catalysts, Catal. Today. 360 (2021) 326–339, https://doi.org/10.1016/j.cattod.2020.02.018.
[25] A. Väliheikki, M. Kärkkäinen, M. Honkanen, O. Heikkinen, T. Kolli, K. Kallinen, M. Huuhtanen, M. Vippola, J. Lahtinen, R.L. Keiski, Deactivation of Pt/SiO_2-ZrO_2 diesel oxidation catalysts by sulphur, phosphorus and their combinations, Appl. Catal. B Environ. 218 (2017) 409–419, https://doi.org/10.1016/J.APCATB.2017.06.068.
[26] N. Fairley, XPS, http://www.casaxps.com.
[27] A. Delebecque, C. Thomas, C.M. Pradier, C. Methivier, E. Coffre, H. Paoli, M. Carre, Reactivity of a hydroxylated alumina surface in the presence of NO diluted in N_2: A PM-IRRAS in situ investigation, J. Phys. Chem. C. 112 (2008) 2964–2971, https://doi.org/10.1021/jp075250h.
[28] M. Kaltchev, W.T. Tysoe, Infrared spectroscopic investigation of thin alumina films: measurement of acid sites and surface reactivity, Surf. Sci. 430 (1999) 29–36, https://doi.org/10.1016/S0039-6028(99)00376-3.
[29] H.C. Yao, H.K. Stepien, H.S. Gandhi, The effects of SO_2 on the oxidation of hydrocarbons and carbon monoxide over Pt/γ-Al_2O_3 catalysts, J. Catal. 67 (1981) 231–236, https://doi.org/10.1016/0021-9517(81)90276-1.
[30] G.S. Şentürk, E.I. Vovk, V.I. Zaikovskii, Z. Say, A.M. Soylu, V.I. Bukhtiyarov, E. Ozensoy, SOx uptake and release properties of TiO_2/Al_2O_3 and BaO/TiO_2/Al_2O_3 mixed oxide systems as NOx storage materials, Catal. Today. 184 (1) (2012) 54–71, https://doi.org/10.1016/j.cattod.2011.12.006.
[31] F.J. Gracia, S. Guerrero, E.E. Wolf, J.T. Miller, A.J. Kropf, Kinetics, operando FTIR, and controlled atmosphere EXAFS study of the effect of sulfur on Pt-supported catalysts during CO oxidation, J. Catal. 233 (2) (2005) 372–387, https://doi.org/10.1016/j.jcat.2005.04.016.
[32] D.E. Gawthrope, A.F. Lee, K. Wilson, Physicochemical properties of Pt-SO_4/Al_2O_3 alkane oxidation catalysts, Phys. Chem. Chem. Phys. 6 (2004) 3907–3914, https://doi.org/10.1039/B402623C.
[33] Y. Er-rouissi, Z. Chabbou, N. Beloued, S. Aqdim, Chemical durability and structural properties of Al_2O_3-CaO-Na_2O-P_2O_5 glasses studied by IR spectroscopy, XRD and SEM, Adv. Mater. Phys. Chem. 07 (2017) 353–363, https://doi.org/10.4236/ampc.2017.710028.
[34] Y. Ma, W. Shen, Y. Yao, Preparation of nanoscale iron (III) phosphate by using ferro-phosphorus as raw material, IOP Conf. Ser. Earth Environ. Sci. 252 (2019) 022032, https://doi.org/10.1088/1755-1315/252/2/022032.
[35] S. Navarro-Jaén, M.Á. Centeno, O.H. Laguna, J.A. Odriozola, Pt/$CePO_4$ catalysts for the WGS reaction: Influence of the water-supplier role of the support on the catalytic performance, J. Mater. Chem. A. 6 (35) (2018) 17001–17010, https://doi.org/10.1039/C8TA04603D.
[36] P. Webb, C. Orr, Analytical methods in fine particle technology, Micromeritics Instrument Corporation, Norcross, Ga, 1997.
[37] F. Ambroz, T.J. Macdonald, V. Martis, I.P. Parkin, Evaluation of the BET theory for the characterization of meso and microporous MOFs, Small Methods 2 (11) (2018) 1800173, https://doi.org/10.1002/smtd.v2.1110.1002/smtd.201800173.